Proceedings of IMECE2005
2005 ASME International Mechanical Engineering Congress and Exposition
November 5-11, 2005, Orlando, Florida USA

IMECE2005-80394

A STRESS-DEPENDENT HYSTERESIS MODEL FOR FERROMAGNETIC TRANSDUCER MATERIALS

Ralph C. Smith *
Center for Research in Scientific Computation
Department of Mathematics
North Carolina State University
Raleigh, NC 27695
Email: rsmith@eos.ncsu.edu

Marcelo J. Dapino
Department of Mechanical Engineering
The Ohio State University
Columbus, OH 43210
Email: dapino.1@osu.edu

ABSTRACT

This paper focuses on the development of a model which characterizes the nonlinear and hysteretic stress-dependence inherent to magnetic transducer materials operating in high drive regimes. The model builds upon a previous ferromagnetic characterization framework based on energy analysis at the lattice level in combination with stochastic homogenization techniques. Aspects of the stress-dependent magnetomechanical model are illustrated through comparison with experimental steel data.

INTRODUCTION

As detailed in [3, 4, 5, 10, 11], magnetic transducers are increasingly considered as actuators and sensors for numerous aerospace, aeronautic, automotive, industrial, and biomedical applications. For low to moderate drive levels, the relation between input fields H and stresses σ and the magnetization M and induction B generated in the transducer materials is approximately linear, and linear constitutive relations provide sufficient accuracy for system and control design. However, at the higher drive levels required for many applications, hysteresis and constitutive nonlinearities inherent to the H-M, H-B, σ-M, and σ-B relations must be incorporated in models and model-based control designs to achieve accurate transducer characterization and control specifications. In this paper, we extend the framework of [12, 13], which characterizes the nonlinear and hysteretic H-M and H-B behavior of ferromagnetic materials, to include certain stress-dependent effects. This provides initial coupled magnetomechanical constitutive relations that are suitable for subsequent transducer characterization and control design.

The coupled magnetomechanical behavior of ferromagnetic materials is highly complex and we do not attempt to characterize all manifestations of the phenomenon in this paper. Instead we focus on specific effects which must be accommodated to construct nonlinear constitutive relations as a first step toward characterizing the stress-dependent dynamics of high performance actuators and sensors.

The direct magnetomechanical effect can be broadly categorized as reflecting two cooperative phenomena; (i) the behavior of the anhysteretic magnetization M_{an} or induction B_{an} changes due to a number of mechanisms including stress-dependent behavior of local coercive and effective fields, and (ii) the magnetization M is driven to M_{an} (equivalently, B is driven to B_{an}).

The former attribute is illustrated in Figure 1 with anhysteretic H-B_{an} steel data from [8] collected at fixed stresses ranging from -200 MPa to 200 MPa. An observation which proves important for model development is that the curves cross at different field values depending on the fixed input stress.

Figure 2 illustrates the manner through which application of an applied compressive stress drives the magnetization (or equivalently induction) near positive and negative remanence ($H = 80$ A/m) to B_{an}. As detailed in Pitman [9], a steel specimen was driven to both positive and negative saturation and then held at a constant field value of 80 A/m while compres-

* Address all correspondence to this author.

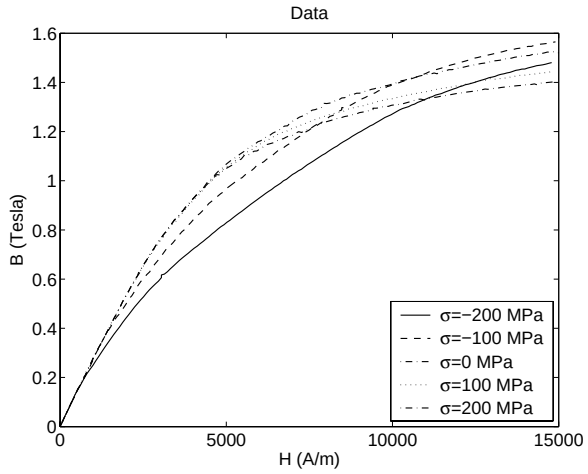

Figure 1. Stress-dependent anhysteretic data from [8].

sive stresses were applied and subsequently released. A comparison of the data plotted in Figures 2(b) and (c) illustrates that in both cases, the induction was driven to B_{an} by input stresses of approximately $\sigma = -400$ MPa. This reflects the fact that these stresses are sufficiently large to eliminate local minima associated with pinning sites so that the induction equilibrates to the global minimum associated with B_{an}. In other words, local coercive fields have been reduced to zero. Close examination of the σ-B relations upon stress release reveals that they are not constant and hence the global energy minimum associated with B_{an} is also stress-dependent.

Additional details regarding the physics associated with the direct magnetomechanical effect, the Villari effect — which constitutes changes in magnetization due to applied stresses — and previous models used to characterize these phenomena can be found in [2, 7, 11].

In the second section, we summarize the framework developed in [12, 13] to characterize hysteresis and constitutive nonlinearities in the H-M and H-B relations. In the first step of the development, Gibbs energy relations at the lattice level are used to quantify the local average magnetization in the presence or absence of thermal relaxation (magnetic after-effects). Secondly, the effects of polycrystallinity, material nonhomogeneities, and variable effective fields are incorporated by treating physical quantities such as the coercive and effective fields as manifestations of underlying distributions rather than fixed parameters. In the third section, we extend this framework to incorporate input stresses through the introduction of generalized Gibbs energy relations and stress-dependent parameters in the homogenized energy framework. Attributes of the model are illustrated in the fourth through fits to the experimental steel data plotted in Figures 1 and 2. We note that whereas steel does not provide the output levels associated with transducer materials such

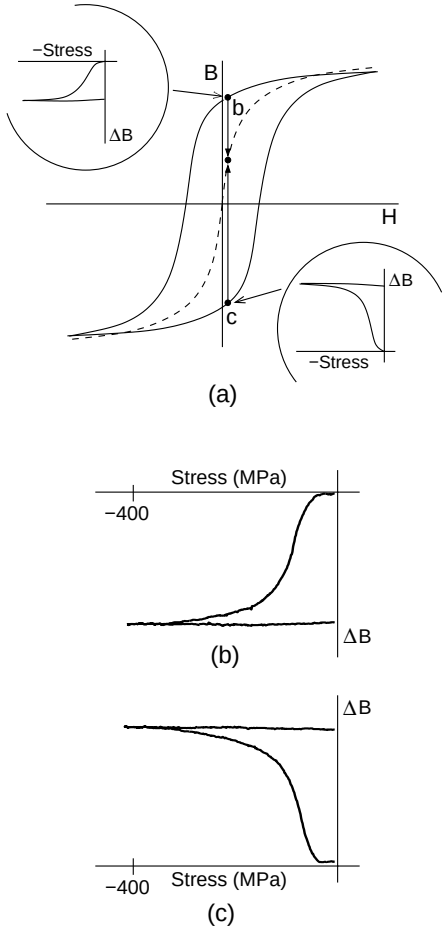

Figure 2. (a) Manner through which the induction near positive remanence is driven to the anhysteretic curve through application of compressive stresses; (b) and (c) data from Pitman [9] quantifying the σ-B behavior for steel near positive and negative remanence.

as Terfenol-D, its magnetomechanical properties have been more widely investigated which facilitates illustration of the model. The framework is equally applicable to more specialized transducer materials such as Terfenol or Galfenol.

MAGNETIC MODEL

As a prelude to the development of a coupled magnetomechanical model for ferromagnetic materials, we summarize first the magnetic model developed in [12, 13]. This model was developed in the context of uniaxial materials but is generally applicable to isotropic and weakly anisotropic materials. The framework provides the capability for incorporating magnetic after-effects and thermal relaxation but does not include eddy current losses; hence it should be employed for low frequency regimes or transducer architectures for which eddy current losses are minimal.

At the lattice level, two Helmholtz energy relations are appropriate. The first,

$$\psi(M,T) = \frac{H_h M_s}{2}\left[1-(M/M_s)^2\right] + \frac{H_h T}{2T_c}\left[M\ln\left(\frac{M+M_s}{M_s-M}\right)+M_s\ln\left(1-(M/M_s)^2\right)\right], \tag{1}$$

results from statistical mechanics principles whereas asymptotic approximation of (1) under fixed temperature conditions yields the piecewise quadratic relation

$$\psi(M) = \begin{cases} \frac{1}{2}\eta(M+M_R)^2 & , M \le -M_I \\ \frac{1}{2}\eta(M-M_R)^2 & , M \ge M_I \\ \frac{1}{2}\eta(M_I-M_R)\left(\frac{M^2}{M_I}-M_R\right) & , |M| < M_I. \end{cases} \tag{2}$$

In (1), H_h, M_s and T_s respectively denote a bias field, the local saturation magnetization, and the Curie temperature whereas M_R, M_I and η in (2) denote a local remanence magnetization, the positive inflection point and the reciprocal of the slope for the hysteresis kernel after moment switching. For simplicity, we will focus on (2) throughout the remainder of this discussion while noting that analogous theory holds for (1) as detailed in [12, 13].

An appropriate expression for the Gibbs energy is

$$G(H,M) = \psi(M) - \mu_0 HM \tag{3}$$

where μ_0 denotes the permeability of free space. The behavior of the Gibbs energy for $H = 0$ and positive applied fields is depicted in Figure 3.

A macroscopic magnetization model is constructed in two steps. In the first, we summarize relations for the local average magnetization $\overline{M}$ in the presence and absence of thermal activation. These relations can be directly extrapolated to quantify the magnetization in homogeneous, isotropic materials with constant effective fields. In the second step of the development, stochastic homogenization techniques based on the tenet that certain material properties are manifestations of underlying distributions rather than constants are employed to construct macroscopic models which incorporate the effects of polycrystallinity, material nonhomogeneities, and variable effective fields.

For regimes in which thermal activation is significant, $\overline{M}$ is given by

$$\overline{M} = x_+ \langle M_+ \rangle + x_- \langle M_- \rangle \tag{4}$$

where x_+, x_- denote the fraction of positively and negatively oriented moments and $\langle M_+ \rangle, \langle M_- \rangle$ are corresponding expected

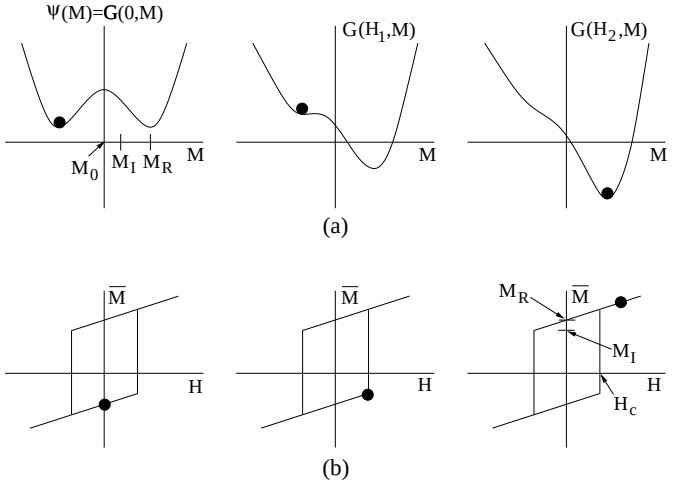

Figure 3. (a) Helmholtz energy ψ and Gibbs energy G for increasing field H ($H_2 > H_1 > 0$). (b) Dependence of the local average magnetization $\overline{M}$ given by (9) or (10) on the field in the absence of thermal activation.

magnetizations. Using the Boltzmann relation

$$\mu(G) = Ce^{-GV/kT}, \tag{5}$$

to quantify the probability of achieving an energy level G, where C, V and k respectively denote an integration constant, a control volume, and Boltzmann's constant, the expected magnetizations $\langle M_+ \rangle$ and $\langle M_- \rangle$ are given by

$$\langle M_+ \rangle = \frac{\int_{M_I}^{\infty} Me^{-G(H,M,T)V/kT}dM}{\int_{M_I}^{\infty} e^{-G(H,M,T)V/kT}dM}$$
$$\langle M_- \rangle = \frac{\int_{-\infty}^{-M_I} Me^{-G(H,M)V/kT}dM}{\int_{-\infty}^{-M_I} e^{-G(H,M)V/kT}dM}. \tag{6}$$

The moment fractions are quantified by the evolution equations

$$\dot{x}_+ = -p_{+-}x_+ + p_{-+}x_-$$
$$\dot{x}_- = -p_{-+}x_- + p_{+-}x_+$$

which can be simplified to

$$\dot{x}_+ = -p_{+-}x_+ + p_{-+}(1-x_+) \tag{7}$$

through the identity $x_+ + x_- = 1$. The likelihoods of switching orientations are

$$p_{+-} = \frac{1}{T\,(T)} \frac{\int_{M_I-\varepsilon}^{M_I} e^{-G(E,M)V/kT}\,dM}{\int_{M_I-\varepsilon}^{\infty} e^{-G(E,M)V/kT}\,dM}$$
$$p_{-+} = \frac{1}{T\,(T)} \frac{\int_{-M_I}^{-M_I+\varepsilon} e^{-G(E,M)V/kT}\,dM}{\int_{-\infty}^{-M_I+\varepsilon} e^{-G(E,M)V/kT}\,dM} \tag{8}$$

where ε is taken to be a small positive constant and T is the relaxation time.

For regimes in which thermal activation is negligible, moments switch instantaneously as compared with the more gradual transitions associated with thermally active operating regimes in which moments can switch in advance of fields which eliminate local minima of G — e.g., see Figure 4.

The kernel in the absence of thermal activation can be determined using the sufficient condition $\frac{\partial G}{\partial M} = 0$ to be

$$\overline{M} = \frac{\mu_0}{\eta} H + M_R \delta \tag{9}$$

where $\delta = 1$ for positively oriented moments and $\delta = -1$ for negative orientations. To quantify δ in terms of initial moment configurations and previous switches, we employ Preisach notation and take

$$[\overline{M}(H;H_c,\xi)](t) = \begin{cases} [\overline{M}(H;H_c,\xi)](0) \\ \frac{\mu_0}{\eta} H - M_R \\ \frac{\mu_0}{\eta} H + M_R \end{cases} \tag{10}$$

for the respective cases $\{\tau(t) = \emptyset\}$, $\{\tau(t) \neq \emptyset \text{ and } H(\max \tau(t)) = -H_c\}$, $\{\tau(t) \neq \emptyset \text{ and } H(\max \tau(t)) = H_c\}$. Here

$$H_c = \frac{\eta}{\mu_0}(M_R - M_I) \tag{11}$$

denotes the local coercive field and

$$\tau(t) = \{t \in (0,t_f]\,|\,H(t) = -H_c \text{ or } H(t) = H_c\}$$

denotes transition points. The initial moment orientation is given

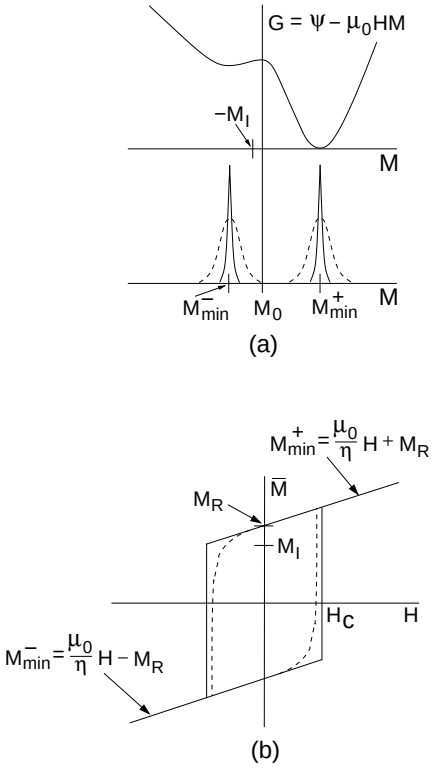

Figure 4. (a) Gibbs energy profile with a high level (– – –) and low level (——) of thermal activation in the Boltzmann probability $\mu(G) = Ce^{-GV/kT}$. (b) Local magnetization $\overline{M}$ given by equation (4) with high thermal activation (– – –) and limiting magnetization $\overline{M}$ specified by (9) or (10) in the absence of thermal activation (——).

by

$$[\overline{M}(H;H_c,\xi)](0) = \begin{cases} \frac{\mu_0}{\eta} H - M_R & , H(0) \leq -H_c \\ \xi & , -H_c < H(0) < H_c \\ \frac{\mu_0}{\eta} H + M_R & , H(0) \geq H_c \end{cases}$$

The behavior of $\overline{M}$ given by (10) in this limiting case is depicted in Figure 3(b) and 4(b).

The kernels $\overline{M}$ given by (4) or (10) quantify the hysteretic behavior at the lattice level and yield macroscopic models only for homogeneous materials with negligible interaction fields H_I — hence the effective field $H_e = H + H_I$ is simply the applied field H.

To incorporate the effects of polycrystallinity, material nonhomogeneities, inclusions, texture, and variable interaction fields, we make the assumption that the local coercive field H_c given by (11) and interaction field H_I are stochastically distributed with respective densities ν_1 and ν_2 which satisfy the de-

cay criteria

$$\begin{aligned}&\text{(i)}\quad \nu_1(x)\ \text{ defined for } x>0,\\ &\text{(ii)}\quad \nu_2(-x)=\nu_2(x),\\ &\text{(iii)}\quad |\nu_1(x)|\le c_1e^{-a_1x}\quad,\quad |\nu_2(x)|\le c_2e^{-a_2|x|}\end{aligned}$$

for positive c_1, a_1, c_2, a_2. These assumptions enforce the physical properties that local coercive fields are positive, low-field Rayleigh loops are symmetric [1], and local coercive and interaction fields decay as a function of distance. As detailed in [11, 12, 13], one choice for ν_1 and ν_2 which facilitates implementation and provides sufficient accuracy for various materials and applications is

$$\begin{aligned}\nu_1(H_c) &= c_1e^{-[\ln(H_c/\overline{H}_c)/2c]^2}\\ \nu_2(H_I) &= c_2e^{-H_I^2/2b^2}\end{aligned} \tag{12}$$

where c_1, c_2, b are positive constants and $\langle H_c\rangle \approx \overline{H}_c$ approximates the mean of the lognormal distribution when c is small compared with $\overline{H}_c$.

The resulting macroscopic magnetization model is

$$M(H)=\int_0^\infty\int_{-\infty}^\infty \nu_1(H_c)\nu_2(H_I)\overline{M}(H+H_I;H_c,\xi)]\,dH_I\,dH_c \tag{13}$$

with $\overline{M}$ given by (4) or (10). Approximation of the integrals in (13) yields

$$M(H)=\sum_{i=1}^{N_i}\sum_{j=1}^{N_j}\nu_1(H_{c_i})\nu_2(H_{I_j})\overline{M}(H_{I_j}+H;H_{c_i},\xi_j)v_iw_j \tag{14}$$

where H_{I_j}, H_{c_i} are abscissas and v_i, w_j are quadrature weights. Details regarding the construction, implementation, and accuracy of (14) for various ferromagnetic materials can be found in [11, 12, 13].

MAGNETOMECHANICAL MODEL

To extend the framework of the last section to include the direct magnetomechanical effects illustrated in Figures 1 and 2, we consider two extensions to the theory: (i) formulation of a more general Gibbs energy which incorporates magnetomechanical coupling, and (ii) development of stress-dependent relations for the mean $\overline{H}_c(\sigma)$ employed in the density definition (12).

Gibbs Energy

To incorporate the stress-dependent effects on the anhysteretic induction B_{an} shown in Figure 1, we extend the Gibbs relation (3) to

$$\begin{aligned}G(H,M,\sigma,\varepsilon) = \psi(M)+\gamma_4M^4+\frac{1}{2Y^M}\sigma^2-\gamma_1(\sigma)\sigma M^2\\ -\gamma_2(\sigma)\sigma M^4-\mu_0HM-\sigma\varepsilon\end{aligned} \tag{15}$$

where ψ is given by (2). Here Y^M denotes the Young's modulus at constant magnetization, ε is the uniaxial strain, $\gamma_1(\sigma)$ and $\gamma_2(\sigma)$ are stress-dependent magnetoelastic coupling coefficients, and γ_4 is a constant magnetoelastic coefficient.

For a fixed magnetization level, enforcement of the sufficient condition $\frac{\partial G}{\partial \varepsilon}=0$ yields the nonlinear constitutive relation

$$\sigma = Y^M\varepsilon - Y^M\lambda(\sigma) \tag{16}$$

where

$$\lambda(\sigma)=\gamma_1(\sigma)M^2+\gamma_2(\sigma)M^4 \tag{17}$$

denotes the stress-dependent magnetostriction. Following the approach in Jiles [7], we employ two-term Taylor expansions

$$\begin{aligned}\gamma_1(\sigma) &= \gamma_1(0)+\sigma\gamma_1'(0)\\ \gamma_2(\sigma) &= \gamma_2(0)+\sigma\gamma_2'(0)\end{aligned} \tag{18}$$

for the coupling coefficients. It should be noted that the anhysteretic curves will not cross if $\gamma_2(\sigma)=0$ and hence only quadratic magnetoelastic coupling terms are employed in the Gibbs energy. Moreover, they cross at a single point if $\gamma_1'(0)=\gamma_2'(0)=0$ and hence the magnetostriction is independent of stress. The anhysteretic behavior shown in Figure 1 dictates the retention of all four components. Additionally, the quartic term γ_4M^4 is included to maintain continuity between the internal energy quantified by the Helmholtz energy and the magnetoelastic energy. The coefficients $\gamma_1(0), \gamma_1'(0), \gamma_2(0), \gamma_2'(0)$ and γ_4 are identified through a least squares fit to the data.

For operating regimes in which thermal excitation is sufficient to cause discernible magnetic after-effects, the local magnetization $\overline{M}$ is specified by (4) with the Gibbs relation (15) employed in (6)–(8). For regimes in which thermal activation is negligible, enforcement of the sufficient condition $\frac{\partial G}{\partial M}=0$ yields the stress-dependent magnetization relation

$$\begin{aligned}[4\gamma_4+4\gamma_2(\sigma)\sigma]M^3+[2\gamma_1(\sigma)\sigma-\eta]M\\ +[\mu_0H+\delta\eta M_R]=0.\end{aligned} \tag{19}$$

For model construction, this cubic relation can be solved either directly or using a gradient-based optimization method.

Stress-Dependence of $\overline{H}_c(\sigma)$

The Pitman data plotted in Figure 2 illustrates that the mean $\langle H_c(\sigma)\rangle \approx \overline{H}_c(\sigma)$ is driven to zero by both tensile (positive) and compressive (negative) stresses. It has also been verified that this effect is rate-dependent with higher values of $\left|\frac{d\sigma}{dt}\right|$ causing faster decreases in the local coercive field.

To phenomenologically incorporate these effects, we employ the stress-dependent relation

$$\begin{aligned}\overline{H}_c(\sigma) &= \widehat{H}_c e^{-\left(k+\left|\frac{d\sigma}{dt}\right|\sigma\right)\sigma} \\ &= \widehat{H}_c e^{-(k+k_2\sigma)\sigma}\end{aligned} \tag{20}$$

where $k_2 = \left|\frac{d\sigma}{dt}\right|$. The parameters $\widehat{H}_c, k$ and k_2 are determined through a least squares fit to the data.

MODEL VALIDATION WITH EXPERIMENTAL DATA

Example 1

We first consider the characterization of the Pitman data plotted in Figure 2. As noted in the Introduction and detailed in [9], this data was collected from a steel sample that was driven in two separate experiments to positive and negative saturation and then held at a constant field of 80 A/m while compressive stresses were applied and subsequently released. This had the effect of driving local coercive fields to zero which reduced the magnetization and induction to the anhysteretic values. The slight stress-dependence of the anhysteretic induction B_{an} is noted in the data plotted in Figure 5 as the stress is increased to zero.

To construct the model, the parameters $M_R = 5.4\times10^3$ A/m, $\eta = 2.765\times10^{-6}$, $b = 0.4$ A/m, $c = 19.2\times10^6$ A/m, $C = c_1\cdot c_2 = 0.0323$, $\gamma_1(0) = 1\times10^{-16}$ $\mathrm{A^{-2}m^2}$, $\gamma_1'(0) = -3.51\times10^{-22}$ $\mathrm{A^{-2}m^2Pa^{-1}}$, $\gamma_2(0) = -1.08\times10^{-22}$ $\mathrm{A^{-4}m^4}$, $\gamma_2'(0) = -5.0\times10^{-31}$ $\mathrm{A^{-4}m^4Pa^{-1}}$, $\gamma_4 = -6.0\times10^{-15}$ $\mathrm{A^{-4}m^4}$, $k = 1.0\times10^{-10}$ $\mathrm{Pa^{-1}}$, $k_2 = 3.5\times10^{-17}$ $\mathrm{Pa^{-1}s^{-1}}$ and $\widehat{H}_c = 6.0\times10^3$ A/m were obtained through a fit to the data. The resulting model fit, with induction values computed using the relation $B = \mu_0(H+M)$, is compared with the data in Figure 5 where it is observed that the model accurately quantifies both the reduction in local coercive fields and change anhysteretic behavior associated with application and release of compressive stresses.

Example 2

Secondly, we illustrate the performance of the model for characterizing the stress-dependent anhysteretic behavior shown in Figure 1. The data was collected from a steel specimen having a length of 6 cm and cross-sectional area of 1 cm as reported by Jiles and Atherton [8].

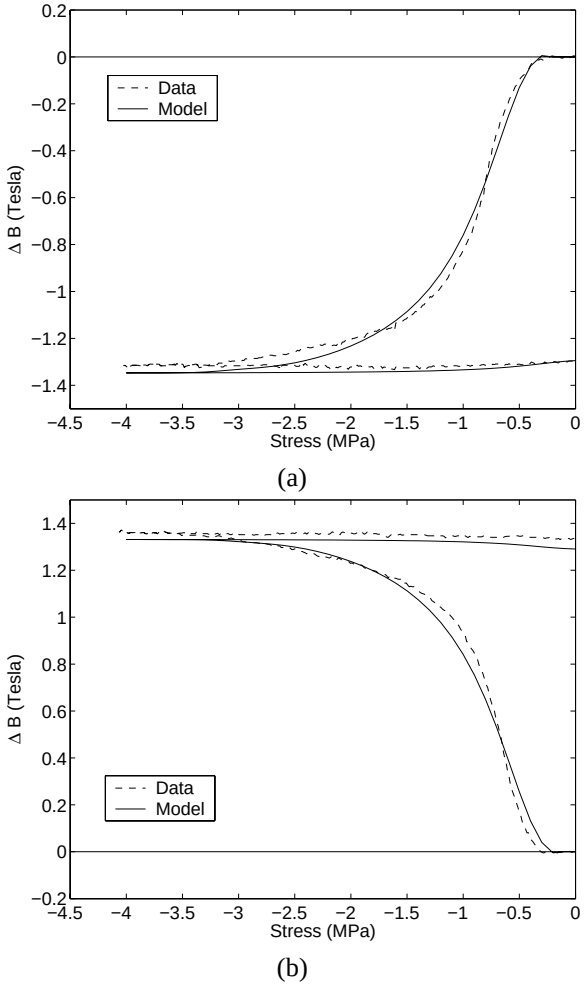

Figure 5. Changes in the induction B due to compressive stresses with an initial field of 80 A/m: (a) positive remanence, and (b) negative remanence.

To construct the discretized magnetization model (14), the parameter values $\eta = 2.765\times10^{-6}$, $b = 1.28$ A/m, $c = 19.0\times10^6$ A/m, $C = c_1\cdot c_2 = 0.0204$, $\gamma_1(0) = 4.15\times10^{-15}$ $\mathrm{A^{-2}m^2}$, $\gamma_1'(0) = -4.0\times10^{-23}$ $\mathrm{A^{-2}m^2Pa^{-1}}$, $\gamma_2(0) = -4.65\times10^{-23}$ $\mathrm{A^{-4}m^4}$, $\gamma_2'(0) = -6.8\times10^{-32}$ $\mathrm{A^{-4}m^4Pa^{-1}}$, $\gamma_4 = -6.6\times10^{-15}$ $\mathrm{A^{-4}m^4}$, $k = 1.0\times10^{-9}$ $\mathrm{Pa^{-1}}$ and $\widehat{H}_c = 4.0\times10^3$ A/m were determined through a fit to the data. We note that $k_2 = \left|\frac{d\sigma}{dt}\right| = 0$ since stresses are fixed in each case. Corresponding induction values were computed using the relation $B = \mu_0(M+H)$. The resulting model fit is compared with the data in Figure 6 where it is observed that the model accurately quantifies the stress-dependent behavior of the anhysteretic magnetization and induction.

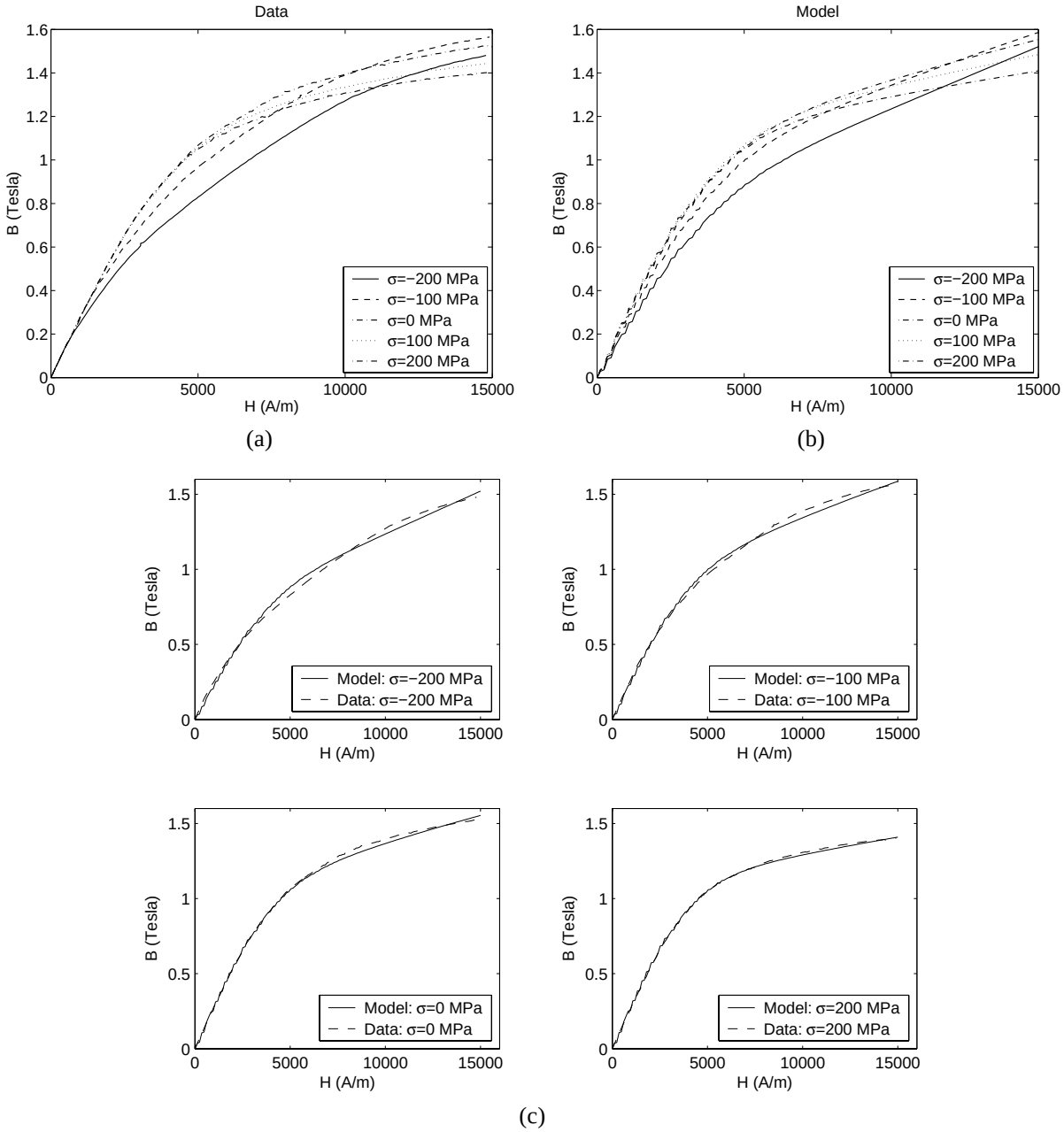

Figure 6. (a) Stress-dependent anhysteretic magnetization data from [8], (b) model predictions given by (13), and (c) comparison between model predictions and experimental data for stresses of -200 MPa, -100 MPa, 0 Mpa and 200 MPa.

CONCLUDING REMARKS

This paper addresses the incorporation of direct magnetomechanical coupling inherent to magnetic materials in a manner which facilitates the development of nonlinear constitutive relations for subsequent transducer and control design. The initial framework for the model is provided by theory from [12, 13] which quantifies the nonlinear and hysteretic behavior of *H-M* and *H-B* relations. Stress-dependence is incorporated by formulation of an extended Gibbs energy relation and stress-dependent coercive field expression. Attributes of the model are illustrated through comparison with experimental steel data. Present investigations are focused on the development and experimental validation of distributed transducer models using these nonlinear constitutive relations.

ACKNOWLEDGMENT

The research of R.C.S. was supported in part through the NSF grants CMS-0099764, CMS-0201560 and in part by the Air Force Office of Scientific Research through the grants AFOSR-F49620-01-1-0107 and AFOSR-FA9550-04-1-0203. The research of M.J.D. was supported in part by Ohio State University.

REFERENCES

[1] Bertotti, G., 1998, *Hysteresis in Magnetism: For Physicists, Materials Scientists, and Engineers*, Academic Press, San Diego, CA.

[2] Chikazumi, S., 1997, *Physics of Ferromagnetism*, Second Edition, English edition prepared with the assistance of C.D. Graham, Jr., Clarendon Press, Oxford.

[3] Dapino, M.J., 2002, "Magnetostrictive materials," *Encyclopedia of Smart Materials*, M. Schwartz, Ed., John Wiley and Sons, New York, pp. 600–620.

[4] Dapino, M.J., 2004, "On magnetostrictive materials and their use in adaptive structures," *International Journal of Structural Engineering and Mechanics*, 17(3-4), pp. 303–329.

[5] Dapino, M.J., Calkins, F.T., and Flatau, A.B., 1999, "Magnetostrictive devices," *Wiley Encyclopedia of Electrical and Electronics Engineering*, John G. Webster, Ed., John Wiley and Sons, Inc., New York, Volume 12, pp. 278–305.

[6] Goodenough, J.B., 2002, "Summary of losses in magnetic materials," *IEEE Transactions on Magnetics*, 38(5), pp. 3398–3408.

[7] Jiles, D.C., 1995, "Theory of the magnetomechanical effect," *Journal of Physics D: Applied Physics*, 28, pp. 1537–1546.

[8] Jiles, D.C., and Atherton, D.L., 1984, "Theory of the magnetisation process in ferromagnetics and its application to the magnetomechanical effect," *Journal of Physics D: Applied Physics*, 17, pp. 1265–1281.

[9] Pitman, K.C., 1990, "The influence of stress on ferromagnetic hysteresis," *IEEE Transactions on Magnetics*, 26(5), pp. 1978–1980.

[10] Restorff, J.B., 1994, "Magnetostrictive materials and devices," *Encyclopedia of Applied Physics*, Volume 9, pp. 229–244.

[11] Smith, R.C., 2005, *Smart Material Systems: Model Development*, SIAM, Philadelphia, PA.

[12] Smith, R.C., Dapino, M.J., Braun, T.R., and Mortensen, A.P., 2005, "A homogenized energy framework for ferromagnetic hysteresis," *IEEE Transactions on Magnetics*, submitted.

[13] Smith, R.C., Dapino, M.J., and Seelecke, S., 2003, "A free energy model for hysteresis in magnetostrictive transducers," *Journal of Applied Physics*, 93(1), pp. 458–466.